Available online at www.sciencedirect.com
SCIENCE DIRECT®
Combustion and Flame 143 (2005) 549–565
Combustion and Flame
www.elsevier.com/locate/combustflame

Effect of dilatation on scalar dissipation in turbulent premixed flames

N. Swaminathan *, K.N.C. Bray

Department of Engineering, University of Cambridge, Cambridge CB2 1PZ, UK

Received 21 February 2005; received in revised form 28 August 2005; accepted 31 August 2005

Available online 10 October 2005

Abstract

The scalar dissipation rate signifies the local mixing rate and thus plays a vital role in the modeling of reaction rate in turbulent flames. The local mixing rate is influenced by the turbulence, the chemical, and the molecular diffusion processes which are strongly coupled in turbulent premixed flames. Thus, a model for the mean scalar dissipation rate, and hence the mean reaction rate, should include the contributions of these processes. Earlier models for the scalar dissipation rate include only a turbulence time scale. In this study, we derive exact transport equations for the instantaneous and the mean scalar dissipation rates. Using these equations, a simple algebraic model for the mean scalar dissipation rate is obtained. This model includes a chemical as well as a turbulence time scale and its prediction compares well with direct numerical simulation results. Reynolds-averaged Navier–Stokes calculations of a test flame using the model obtained here show that the contribution of dilatation to local turbulent mixing rate is important to predict the propagation phenomenon.

Keywords: Scalar dissipation; Premixed flame modeling; Heat release effect

1. Introduction

In turbulent combustion modeling, the closure of reaction rate is challenging as it involves a nonlinear expression. But this challenging problem can be simplified to a tractable form if one assumes the reaction zones to be thin compared to a typical fluid dynamic scale (Kolmogorov length scale) [1]. The thin flame assumption makes it possible to approximate the probability density function of a reaction progress variable, c, by a double delta function, representing the unburnt and burnt mixtures [2]. This approximation leads to many attractive simplifications of the turbulent premixed flame problem. The progress variable may be defined using any reactive scalars, but commonly temperature is used. Alternative propositions for the choice of variables to define c are also made [3]. Here, we define the progress variable as $c \equiv (T - T_u)/(T_b - T_u)$, where T is the absolute temperature, and subscripts u and b respectively denote unburnt and burnt mixtures. The instantaneous c is governed by

$$\rho \frac{\mathrm{D}c}{\mathrm{D}t} = \dot{\omega} + \mathcal{D}, \tag{1}$$

where ρ is the fluid density and $\mathrm{D}/\mathrm{D}t$ is the total derivative $(\partial/\partial t + u_j \partial/\partial x_j)$ representing the temporal and convective changes of c inside a control volume. Symbols t, x_j, and u_j respectively denote time, spatial coordinate in direction j, and the com-

* Corresponding author.
E-mail address: ns341@cam.ac.uk (N. Swaminathan).

0010-2180/$ – see front matter
doi:10.1016/j.combustflame.2005.08.020

ponent of fluid velocity in that direction. The first term on the right-hand side, $\dot{\omega}$, is the chemical source term and the second term represents the diffusive flux of c, $\mathcal{D} \equiv \partial[\rho\alpha\partial c/\partial x_j]/\partial x_j$ with α as the diffusivity of c. Here and in the following discussion, repeated indices imply summation over them. In an engineering calculation, a balance equation for $\tilde{c}$ is solved [1]. The mass-weighted average, also known as the Favre average, of c is denoted by $\tilde{c}$ and the fluctuation over this average is c''. The contributions of chemical reaction, $\overline{\dot{\omega}}$, and the turbulent flux, $\widetilde{u''c''}$, to the $\tilde{c}$ balance equation need to be modeled.

With the thin flame assumption, the average reaction rate, $\overline{\dot{\omega}}$, may be modeled [1] as the product of mean reaction rate per unit flame surface area and the flame surface density, Σ. Thus, $\overline{\dot{\omega}} = (\rho_u s_L^o I_o)\Sigma$, where ρ_u is unburnt mixture density, s_L^o is unstretched laminar burning velocity, and I_o represents the effect of flame stretch on the laminar burning velocity. This effect is captured via a correlation involving Karlovitz and Markstein numbers [4]. It is apparent from the above expression that the amplification of reaction rate by turbulence is predominantly represented by Σ. Various forms of the $\overline{\dot{\omega}}$ model proposed in earlier studies are discussed by Veynante and Vervisch [6].

Various approaches have been followed to model Σ. The Bray–Moss–Libby (BML) [5] approach yields an algebraic expression for Σ. In an another approach, a balance equation for Σ is solved [7]. The balance equation for Σ is postulated by Marble and Broadwell [8] and rigorously derived from fundamental principles by Pope [9] and Candel and Poinsot [10]. The flame surface density, Σ, can also be related to scalar dissipation rate of the progress variable, $N \equiv \alpha(\nabla c \cdot \nabla c) = \alpha(c_{,k}\, c_{,k})$. It has been shown [11] that $\widetilde{\epsilon_c} = K_\Sigma s_L \Sigma$, where $\widetilde{\epsilon_c} = \widetilde{\alpha(\nabla c'' \cdot \nabla c'')}$ and K_Σ is a constant. The quantity $\widetilde{\epsilon_c}$ is the dissipation rate of progress variable variance. In the thin flame regime [11] $\tilde{c}_{,k} \ll c''_{,k}$.

Pope [21] deduced the surface density function of an iso-surface $c = \zeta$ to be $\Sigma_p(\zeta; \mathbf{x}, t) = \langle\sqrt{N/\alpha}|c = \zeta\rangle\ P_c(\zeta)$ without invoking the assumption of thin flame. There should not, however, be any local extinction on the surface $c = \zeta$ as this would invalidate the continuity of c on the particular surface. The quantity within the angle bracket denotes conditional average and P_c is the marginal pdf of c. The conditional average, N_ζ, is defined as the ensemble average of those samples satisfying the condition $c = \zeta$. The flame surface density Σ can be obtained from the surface density function Σ_p either by choosing a particular value of ζ or by averaging [6] $\overline{\Sigma} = \int \Sigma_p\, \mathrm{d}\zeta$. Under the assumption of thin flamelets one gets $\Sigma \simeq \overline{\Sigma}$.

In the above discussion, one sees that the scalar dissipation rate is related to the flame surface density and to the reaction rate. Borghi and his co-workers [11–14] have studied a balance equation for $\widetilde{\epsilon_c}$. In these works, the effect of heat release has been ignored by treating fluid density as constant. In this work, we follow a simple method to derive the scalar dissipation rate equation including the heat-release effects and obtain a simple model for $\widetilde{\epsilon_c}$. It can also be noted that the $\widetilde{\epsilon_c}$ transport equation can be related to the Σ equation in the thin flamelet regime. One needs an evolution equation for $N_\zeta \equiv \langle N|\zeta\rangle$ to obtain the Σ equation via Σ_p. The flame surface density equation obtained via Σ_p may be applicable to not only the thin flame but also to thickened flames. Here, we confine ourselves to the thin flamelet regime and concentrate on obtaining a simple model for $\widetilde{\epsilon_c}$.

In the next section, we drive an exact transport equation for the instantaneous scalar dissipation rate, N, and then obtain Borghi's equation by invoking the approximations used in [11–14]. In Section 2.3, a simple model for $\widetilde{\epsilon_c}$ involving the chemical and turbulence time scales is obtained. Direct numerical simulation (DNS) data sets [15,16] are analyzed in Section 3 to validate the model developed here. Results from a Reynolds-averaged Navier–Stokes simulation (RANS) of a simple test problem are discussed in Section 4 where they are used to compare the predictions of the models obtained here and by Mantel and Borghi [12]. The final section provides a summary and conclusion of this study.

2. Scalar dissipation rate

The scalar dissipation rate, N, characterizing turbulent mixing is an important quantity in turbulent reacting flows. It is directly related to the heat-release rate in premixed [17,18] as well as in nonpremixed [19,20] flames. It is also involved in flamelet [20], probability density function [21], and conditional moment closure [22] models of turbulent combustion. A wealth of information on the scalar dissipation rate of mixture fraction, which is a chemically conserved scalar, is available in the literature [6,23–25]. However, the information on N in turbulent premixed flames is limited. Modeling of N using the turbulent time scale alone, as is done in [4] for nonpremixed flames, is insufficient for premixed flames. The influence of chemical processes should also be considered (see Eq. (13) below) because of strong coupling among the turbulence, the chemical, and the molecular diffusion processes in turbulent premixed flames.

Few experimental studies [26–29] have been carried out to understand the behavior of N. These studies, except [28], show that the values of N in turbulent premixed flames are low compared to laminar flame values. Analysis [30] of direct numerical simulation

results shows an increase in N compared to laminar values. More detailed investigations are required to reconcile these differences. This reconciliation is not intended here but will be the subject of future work. It is anticipated that the framework set out here will help such an investigation. In the following subsection we derive a transport equation for N from Eq. (1).

2.1. Governing equation for N

Khajeh-Nouri [31] and Zeman and Lumley [32] derived a transport equation for $\widetilde{\epsilon_c}$ for buoyancy-driven mixing layer studies. In those studies, the fluid density is treated as a constant but a Bousinesq approximation is used to account for buoyancy effects. Jones and Musonge [33] also used such an equation to model a variety of high Reynolds number turbulent flows including mean scalar gradients. Borghi and Dutoya [13] derived this transport equation with constant density assumption for chemically reacting flows. Recently, a Favre form of this equation is also presented in [14]. The details of the derivation may be found in [11–13]. It is suggested in [14] that some of the effects of density change across the flame front can be incorporated via Landau–Darrieus instabilities following Paul and Bray [34]. The model of Paul and Bray [34] is a phenomenological one and accounts for the effects of density change only when the ratio of root-mean-square value of turbulence fluctuating velocity to unstrained laminar flame propagation velocity is low. Here, we follow a simple approach [35,36] which automatically accounts for the density change across the flame front. This equation is applicable to all turbulent premixed combustion regimes. However, we limit our analysis to turbulent combustion in the thin flamelet regime characterized by $\mathrm{Da} \gg \sqrt{\mathrm{Re}}$. The turbulence Reynolds, Re, and Damköhler, Da, numbers are defined later in Section 2.2.

First, we obtain a governing equation for $c_{,k}$ by differentiating Eq. (1) in direction k. This equation is

$$\rho \frac{\mathrm{D}c_{,k}}{\mathrm{D}t} + \rho u_{j,k} c_{,j} + \frac{\rho_{,k}}{\rho}[\dot{\omega} + \mathcal{D}] = \dot{\omega}_{,k} + \mathcal{D}_{,k}\,. \quad (2)$$

Note that Eq. (1) is used again to obtain the part within the square bracket in the third term. The second term represents the interaction of scalar and flow fields via their respective gradients. The tensor term, $u_{j,k}$, can also be written as the sum of strain ($e_{jk} = 0.5(u_{j,k} + u_{k,j})$) and rotation ($r_{jk} = 0.5(u_{j,k} - u_{k,j})$) tensors.

If the progress variable is defined in terms of temperature, then it can be shown [4,30] that $\rho_u = \rho(1 + \tau c)$ and $\tau[\dot{\omega} + \mathcal{D}] = \rho_u(\partial u_l/\partial x_l)$, by using the state and continuity equations for low Mach number combustion. The heat release parameter τ is defined as $\tau \equiv (T_b - T_u)/T_u$. The second part relating the dilatation, $(\partial u_l/\partial x_l)$, to reaction rate and diffusion is known as the dilatation equation [30]. By using the above expressions, it can be shown that

$$\frac{\rho_{,k}}{\rho}[\dot{\omega} + \mathcal{D}] = -\rho c_{,k}\left(\frac{\partial u_l}{\partial x_l}\right). \quad (3)$$

Multiplying Eq. (2) by $2\alpha c_{,k}$ one obtains

$$\begin{aligned}\rho \frac{\mathrm{D}N}{\mathrm{D}t} = {} & \frac{\partial}{\partial x_j}\left(\rho\alpha\frac{\partial N}{\partial x_j}\right) - 2\rho\alpha\alpha\frac{\partial c_{,k}}{\partial x_j}\frac{\partial c_{,k}}{\partial x_j} \\ & - 2\rho\alpha c_{,j}\, e_{jk} c_{,k} + 2\rho N\left(\frac{\partial u_l}{\partial x_l}\right) \\ & + 2\alpha c_{,k}\,\dot{\omega}_{,k} + c_{,k}^2\,\mathcal{F}(\alpha), \end{aligned} \quad (4)$$

as a governing equation for the instantaneous scalar dissipation rate, N. The contribution from the rotation tensor, r_{jk}, will be zero and thus only the strain part, e_{jk}, appears above. The diffusivity of c is treated as temperature dependent and its contribution is lumped into $\mathcal{F}(\alpha)$ which is given by

$$\begin{aligned}\mathcal{F}(\alpha) \equiv {} & \left\{\rho\frac{\mathrm{D}\alpha}{\mathrm{D}t} - \frac{\partial}{\partial x_j}\left(\rho\alpha\frac{\partial\alpha}{\partial x_j}\right)\right\} \\ & - 4\rho\alpha\frac{\partial \ln(c_{,k})}{\partial x_j}\frac{\partial\alpha}{\partial x_j} \\ & + 2\frac{\alpha}{c_{,k}}\frac{\partial}{\partial x_j}\left(\frac{\partial c}{\partial x_j}\frac{\partial\rho\alpha}{\partial x_k}\right). \end{aligned}$$

It should also be noted that there is a term involving the derivative of density gradient resulting from $2\alpha c_{,k}\mathcal{D}_{,k}$. We expect this term to be small compared to other terms and thus it is included in $\mathcal{F}(\alpha)$ as the last term.

The meaning of various terms in Eq. (4) is as follows. The left-hand side represents the temporal and convective changes of N. The first term on the right-hand side is the diffusive flux term. The second term denotes the dissipation of N. The third term represents the interaction of turbulence and scalar fields. The fourth term represents the source or sink for production of N due to chemical and diffusive processes undergone by c. This term appears because density is allowed to vary across the flame front. The source or sink nature of this term depends on the sign of the correlation between the scalar dissipation rate and the dilatation. Since c is a reactive scalar, the usual production of N because of chemical reaction is represented by the fifth term. The last term is because of the temperature dependence of the thermal diffusivity of the mixture, which is expected to be small compared to the rest of the terms in Eq. (4). As one may see in Eq. (4), the effects of density change appears naturally via the fourth term.

The equation used in earlier studies [11–14,31,32] is for $\widetilde{\epsilon_c}$. The instantaneous N may be written as a sum of Favre mean and fluctuation, viz., $N = \widetilde{N} + n''$. By using the definitions of N and $\widetilde{\epsilon_c}$ given above, one

can write

$$\overline{\rho}\widetilde{\epsilon_c} = \overline{\rho}\widetilde{N} - \overline{\rho\alpha}\left(\tilde{c}_{,k}\,\tilde{c}_{,k}\right). \tag{5}$$

The Favre fluctuation of N is given as $n'' = 2\alpha\tilde{c}_{,k}\,c''_{,k} + \alpha c''_{,k}\,c''_{,k} - \widetilde{\epsilon_c}$. A transport equation for $\widetilde{N}$ can be obtained from Eq. (4) by substituting $N = \widetilde{N} + n''$ and then taking the Favre average and noting $\widetilde{n''} = 0$. This equation may be written as

$$\begin{aligned}\frac{\partial\overline{\rho}\widetilde{N}}{\partial t} &+ \frac{\partial}{\partial x_j}\left(\overline{\rho}\widetilde{U}_j\widetilde{N}\right) - \frac{\partial}{\partial x_j}\left(\overline{\rho\alpha}\frac{\partial\widetilde{N}}{\partial x_j}\right)\\ &= -\frac{\partial\overline{\rho}\widetilde{u''_j n}}{\partial x_j} - 2\overline{\rho\alpha\alpha\frac{\partial c_{,k}}{\partial x_j}\frac{\partial c_{,k}}{\partial x_j}}\\ &\quad - 2\overline{\rho\alpha(c_{,j}\,e_{jk}c_{,k})} + 2\overline{\rho N\left(\frac{\partial u_l}{\partial x_l}\right)}\\ &\quad + 2\overline{\alpha c_{,k}\,\dot{\omega}_{,k}} + \overline{c^2_{,k}\,\mathcal{F}(\alpha)}.\end{aligned} \tag{6}$$

A balance equation for $\tilde{c}_{,k}$ can be obtained by taking the Favre average of Eq. (2). Then the resulting equation is multiplied by $2\tilde{\alpha}\tilde{c}_{,k}$ to obtain a transport equation for $\overline{\rho\alpha}(\tilde{c}_{,k}\,\tilde{c}_{,k})$. This resultant equation is then subtracted from $\widetilde{N}$ equation to obtain a transport equation for $\widetilde{\epsilon_c}$. This equation is written as

$$\begin{aligned}\frac{\partial\overline{\rho}\widetilde{\epsilon_c}}{\partial t} &+ \frac{\partial}{\partial x_j}\left(\overline{\rho}\widetilde{U}_j\widetilde{\epsilon_c}\right) - \frac{\partial}{\partial x_j}\left(\overline{\rho\alpha}\frac{\partial\widetilde{\epsilon_c}}{\partial x_j}\right)\\ &+ 2\overline{\rho\alpha\alpha\left(\frac{\partial c''_{,k}}{\partial x_j}\frac{\partial c''_{,k}}{\partial x_j}\right)} = T_1 + T_2 + T_3 + T_4,\end{aligned} \tag{7}$$

where

$$T_1 \equiv -\frac{\partial\overline{\rho u''_j\epsilon_c}}{\partial x_j} - 2\overline{\rho\alpha}\widetilde{\left(u''_j c''_{,k}\right)}\frac{\partial\tilde{c}_{,k}}{\partial x_j} = T_{11} + T_{12},$$

$$T_2 \equiv 2\overline{\rho}\widetilde{\epsilon_c}\frac{\partial\widetilde{U}_l}{\partial x_l} + 2\overline{\rho\alpha\left(c''_{,k}\,c''_{,k}\frac{\partial u''_l}{\partial x_l}\right)} = 2\overline{\rho\epsilon_c\frac{\partial u_l}{\partial x_l}},$$

$$\begin{aligned}T_3 \equiv &-2\overline{\rho\alpha}\frac{\partial\tilde{c}}{\partial x_j}\widetilde{\left(\frac{\partial c''}{\partial x_k}\frac{\partial u''_j}{\partial x_k}\right)} - 2\overline{\rho\alpha}\widetilde{\left(\frac{\partial c''}{\partial x_j}e''_{jk}\frac{\partial c''}{\partial x_k}\right)}\\ &- 2\overline{\rho\alpha}\widetilde{\left(\frac{\partial c''}{\partial x_j}\frac{\partial c''}{\partial x_k}\right)}e_{jk} = T_{31} + T_{32} + T_{33},\end{aligned}$$

$$T_4 \equiv 2\overline{\left(\alpha\frac{\partial c''}{\partial x_k}\frac{\partial\dot{\omega}''}{\partial x_k}\right)},$$

with the contribution of $\mathcal{F}(\alpha)$ ignored. For comparison, we also quote the corresponding equation from Mura and Borghi [14], which is

$$\begin{aligned}\frac{\partial\overline{\rho}\widetilde{\epsilon_c}}{\partial t} &+ \frac{\partial}{\partial x_j}\left(\overline{\rho}\widetilde{U}_j\widetilde{\epsilon_c}\right)\\ &= \underbrace{\frac{\partial}{\partial x_j}\left(\overline{\rho\alpha}\frac{\partial\widetilde{\epsilon_c}}{\partial x_j}\right)}_{\text{(III)}} - \underbrace{\frac{\partial}{\partial x_j}\left(\overline{\rho u''_j\epsilon_c}\right)}_{\text{(IV)}}\\ &\quad \underbrace{- 2\frac{\partial\tilde{c}}{\partial x_j}\overline{\rho\alpha\frac{\partial c''}{\partial x_k}\frac{\partial u''_j}{\partial x_k}}}_{\text{(V)}} \underbrace{- 2\overline{\rho\alpha\frac{\partial c''}{\partial x_j}\frac{\partial c''}{\partial x_k}\frac{\partial\widetilde{U}_j}{\partial x_k}}}_{\text{(VI)}}\\ &\quad \underbrace{- 2\overline{\rho\alpha u''_j\frac{\partial c''}{\partial x_k}\frac{\partial^2\tilde{c}}{\partial x_j\partial x_k}}}_{\text{(VI-b)}} \underbrace{- 2\overline{\rho\alpha\frac{\partial c''}{\partial x_j}\frac{\partial c''}{\partial x_k}\frac{\partial u''_j}{\partial x_k}}}_{\text{(VII)}}\\ &\quad \underbrace{- 2\overline{\rho\alpha\alpha\frac{\partial^2 c''}{\partial x_j\partial x_k}\frac{\partial^2 c''}{\partial x_j\partial x_k}}}_{\text{(VIII)}} \underbrace{+ 2\overline{\alpha\frac{\partial c''}{\partial x_k}\frac{\partial\dot{\omega}''}{\partial x_k}}}_{\text{(IX)}}\end{aligned}$$

in our notation.

If one invokes a constant density approximation ($\partial u_l/\partial x_l = 0$) the equation given in Refs. [12,14] is recovered as above. With this constant density approximation, the third and fourth terms on the left-hand side of Eq. (7) respectively represent terms (III) and (VIII) above. The term T_1 represents the sum of (IV) and (VI-b). The T_2 term is zero because the dilatation is zero when the density is assumed to be constant. Thus, this contribution is absent in the equation of Mura and Borghi. The effects of mean and fluctuating strain fields are lumped into T_3 in Eq. (7). This term represents the sum of (V), (VI), and (VII). The term T_4 represents the (IX) above. Note that the algebraic sign is also included in the T_i terms above. One should also note that Eq. (7) is exact, except for the neglect of $\mathcal{F}(\alpha)$, for turbulent premixed flames but it is unclosed.

2.2. Behavior at high Reynolds and Damköhler numbers limit

The turbulence Reynolds and Damköhler numbers are respectively defined as $\mathrm{Re} \equiv u'\Lambda/\nu_u$ and $\mathrm{Da} \equiv (\tau_f/\tau_c) = \Lambda s_L^o/(u'\delta_L^o)$, where u' is the root-mean-square value of turbulence velocity, Λ is the integral length scale of the turbulence field, δ_L^o is the thermal thickness of unstrained laminar flame, and ν_u is the kinematic viscosity of reactant mixture. Also, we take $\nu_u \simeq \alpha_u$. In the case of thin flames, the gradient of c is zero outside the flame. Thus, the laminar flame scales are used to scale the quantities involving or multiplied by the gradient of c in the order of magnitude analysis. The spatial derivatives of mean quantities are scaled by the integral length scale and the evolution time t is scaled by the eddy turnover time. Details of the order of magnitude analysis of Eq. (7) are given in Appendix A. The following observations can be made from the order of magnitude analysis.

(a) When Re and Da become very large, at the leading order the dissipative term (fourth term on the

LHS of Eq. (7)) is balanced by the dilatation (T_2), the interaction of turbulent strain and scalar gradient (T_{32}), and the chemistry (T_4) terms. It is interesting to note that the dilatation term is coming out naturally as an important term as one would expect in flames. This is contrary to the findings in [35] where the dilatation-related term is deemed to be of lower order.

(b) The temporal, convective, turbulent flux (T_{11}) and the mean strain related term (T_{33}) also become significant when Re is very large but Da is finite. The turbulent flux becoming large compared to the molecular flux is consistent with the traditional high Re assumption.

(c) Mantel and Borghi [12] showed that the production of dissipation rate (T_{12}) due to the interaction of turbulent flux of $c_{,k}$ and its mean gradient scales as $\mathrm{Re}^{-1/2}\,\mathrm{Da}^{-3/2}$ whereas here it scales as $\mathrm{Re}^{-1}\,\mathrm{Da}^{-1}$. This is because of the difference in the scaling of the turbulent flux, $\widetilde{u''c''_{,k}}$. It is scaled as (u'/δ_L^o) in [12] whereas here it is scaled as (s_L^o/δ_L^o). Nevertheless, this term becomes negligible in the thin flamelet combustion regime.

(d) Also, the mean scalar gradient-related term, T_{31}, scales as $\mathrm{Da}^{-3/2}$ in [12] but here it scales as $\mathrm{Re}^{-1/2}\,\mathrm{Da}^{-1/2}$. This difference is because of the scaling used for the fluctuating strain field. Here, $e''_{jk} \sim (s_L^o/\delta_L^o)$, whereas in [12] it is scaled as (u'/λ), with λ as the Taylor length scale. The validity of the scalings used in this study may be adjudged from the results presented in Section 4.1.

(e) More importantly, the interaction of turbulent strain and scalar gradient term, T_{32}, is $\mathcal{O}(1)$ here but in [12] it is $\mathcal{O}(\mathrm{Re}^{1/2}\,\mathrm{Da}^{-1})$. This difference is again because of the scaling difference noted in (c) above.

Based on the order of magnitude analysis discussed above, we will not consider T_{12} further and this neglect is also consistent with $\tilde{c}_{,k} \ll c''_{,k}$ in a thin flamelet combustion regime. Now, Eq. (7) may be written as

$$\overline{\rho}\frac{\mathrm{D}\widetilde{\epsilon_c}}{\mathrm{D}t} = T_{11} + T_2 + T_3 + T_4^*, \tag{8}$$

with

$$T_4^* = T_4 - 2\overline{\rho\alpha\alpha\left(\frac{\partial c''_{,k}}{\partial x_j}\frac{\partial c''_{,k}}{\partial x_j}\right)} + \frac{\partial}{\partial x_j}\left(\overline{\rho\alpha}\frac{\partial\widetilde{\epsilon_c}}{\partial x_j}\right).$$

A simple model for the dissipation rate of the progress variable may be obtained by considering dominant terms in the above equation. We shall do this after identifying appropriate models for various terms on the RHS of Eq. (8) and observing that the chemical time scale also plays a role. Earlier models [4,40] for $\widetilde{\epsilon_c}$ include only the turbulence time scale.

2.3. Models for different terms in Eq. (8)

For the thin flamelet combustion, one may write Eq. (1) as $\mathbf{n}s_L\rho\cdot\nabla c = \dot{\omega} + \mathcal{D}$ along the flame normal, $\mathbf{n}$, which is pointing toward the product side. From this, one may obtain [12]

$$2\overline{\alpha c_{,k}\dot{\omega}_{,k}} = \left(\widetilde{\overline{\rho}n_j s_L}\widetilde{N}\right)_{,j} - \left(\widetilde{\overline{\rho\alpha}N}_{,j}\right)_{,j} + 2\overline{\rho\alpha\alpha(c_{,n})_{,n}(c_{,n})_{,n}}. \tag{9}$$

This equation may also be written by replacing $\widetilde{N}$ with $\widetilde{\epsilon_c}$ from Eq. (5) if $\tilde{c}_{,k} \ll c''_{,k}$. The dissipation term in Eq. (7) may be written as

$$\begin{aligned}\overline{\rho\alpha\alpha(c_{,k})_{,j}(c_{,k})_{,j}} &= \overline{\rho\alpha\alpha(c_{,n})_{,n}(c_{,n})_{,n}} \\ &+ 4\overline{\rho\alpha\alpha(c_{,n})_{,\xi}(c_{,n})_{,\xi}} \\ &+ 4\overline{\rho\alpha\alpha(c_{,\xi})_{,\xi}(c_{,\xi})_{,\xi}}\end{aligned} \tag{10}$$

by decomposing the gradient along the flame normal and tangents [12]. Local isotropy is assumed in the flamelet tangential directions, ξ_1 and ξ_2. By combining the above two expressions one can obtain $T_4^* \equiv -8\{\overline{\rho\alpha\alpha(c''_{,n})_{,\xi}(c''_{,n})_{,\xi}} + \overline{\rho\alpha\alpha(c''_{,\xi})_{,\xi}(c''_{,\xi})_{,\xi}}\}$. The models proposed in [12,14] are adopted here:

$$T_{11} \simeq \frac{\partial}{\partial x_j}\left(\frac{\mu_t}{Sc_{\epsilon_c}}\frac{\partial\widetilde{\epsilon_c}}{\partial x_j}\right),$$

$$\begin{aligned}T_3 &= T_{31} + T_{32} + T_{33} \\ &\simeq -C_{p_c}\overline{\rho}\left(\frac{\tilde{\epsilon}}{\tilde{k}}\right)\widetilde{u''_j c''}\frac{\partial\tilde{c}}{\partial x_j} + A_e\overline{\rho}\left(\frac{\tilde{\epsilon}}{\tilde{k}}\right)\widetilde{\epsilon_c} \\ &\quad - C_{p_u}\overline{\rho}\widetilde{\epsilon_c}\left(\frac{\widetilde{u''_j u''_k}}{\tilde{k}}\right)\widetilde{e}_{jk},\end{aligned}$$

$$T_4^* \simeq -\frac{2}{3}\beta\overline{\rho}\frac{\widetilde{\epsilon_c}^2}{\widetilde{c''^2}}\left(\frac{3}{2} - C_{\epsilon_c}\frac{s_L}{\sqrt{\tilde{k}}}\right).$$

The model constants in the T_3 term and β are given in [12] and are also listed in Table 2, which is discussed later. The local laminar propagation speed is denoted by s_L and it can vary from one point to another on the surface of instantaneous flame front. In the following discussion, we take $s_L \approx s_L^o$.

The dilatation term, T_2, is modeled using the BML approach [4]. In this approach, the marginal pdf of c is $P(c;\mathbf{x},t) = \alpha^*(\mathbf{x},t)\delta(c) + \beta^*(\mathbf{x},t)\delta(1-c) + \gamma^*(\mathbf{x},t)f(c)$. The dilatation is zero everywhere except inside the flame front. Thus, T_2 must be proportional to γ^*. This yields

$$\begin{aligned}T_2 &= 2\rho_u\left(\frac{s_L^o}{\delta_L^o}\right)^2\gamma^*\int_0^1\left\{\frac{\rho}{\rho_u}\left(\frac{\delta_L^o}{s_L^o}\right)^2 N\nabla\cdot\mathbf{u}\right\}_L^o f(c)\,\mathrm{d}c \\ &= 2K_1\rho_u\left(\frac{s_L^o}{\delta_L^o}\right)^2\gamma^* = 2K_c\bar{\dot{\omega}}\left(\frac{s_L^o}{\delta_L^o}\right)\end{aligned}$$

$$= \frac{4K_c}{(2C_m - 1)} \left(\frac{s_L^o}{\delta_L^o} \right) \overline{\rho} \widetilde{\epsilon_c}, \tag{11}$$

where the subscript L and superscript o are used to denote that the quantities are taken from the unstrained planar laminar flames. The symbols K_c and C_m are respectively defined as

$$K_c = \left(\frac{\delta_L^o}{s_L^o} \right) \frac{\int \{\rho N (\nabla \cdot \mathbf{u})\}_L^o f(c)\, \mathrm{d}c}{\int \dot{\omega}_L^o(c) f(c)\, \mathrm{d}c}$$

and

$$C_m = \frac{\int c \dot{\omega}_L^o f(c)\, \mathrm{d}c}{\int \dot{\omega}_L^o f(c)\, \mathrm{d}c}.$$

The symbol $\dot{\omega}_L^o$ represents the mass production rate of c in unstrained laminar flames. Bray [17] has shown that the value of C_m varies from 0.69 to 0.72 for meaningful forms of $f(c)$. Here, we take $C_m = 0.7$. Also, one obtains $K_c \simeq 0.1$ for a uniform distribution of burning mode pdf $f(c)$ and the laminar flame structure obtained via a single irreversible reaction with large activation energy. The use of multistep chemical kinetics to represent the laminar flame structure assumed in the above model will definitely influence the variation of dilatation in the flame front and thus the value of K_c. However, this is a matter of calibration of K_c. Here, we concentrate to achieve our objective of finding a simple algebraic model for the $\widetilde{\epsilon_c}$ involving the chemical and turbulence time scales. The effect of strain and curvature on the correlation, $\overline{N(\nabla \cdot \mathbf{u})}$, is unknown at this time. However, it is observed [37] that the effect of strain on the dilatation is negligible for hydrocarbon and rich hydrogen flames. It is expected that the influence of strain and curvature will come via N. This can also have an influence on the value of K_c.

A simple model for the dissipation rate can now be obtained by considering $\mathcal{O}(1)$ terms in Eq. (7) as noted earlier. If the dilatation term is ignored then $T_{32} + T_4^* \simeq 0$. From this expression and for $(\sqrt{\tilde{k}}/s_L^o) > 2C_{\epsilon_c}/3$, one obtains

$$\widetilde{\epsilon_c} \simeq \left(1 + \frac{2}{3} C_{\epsilon_c} \frac{s_L^o}{\sqrt{\tilde{k}}} \right) C_D \left(\frac{\tilde{\epsilon}}{\tilde{k}} \right) \widetilde{c''^2}, \tag{12}$$

where C_D is the ratio of A_e to β. If the scalar is nonpropagative ($s_L^o = 0$) then one recovers the classical form [4,40]. The additional contribution is because of the curvature produced by the propagating mechanism [9]. It is also important to note that the chemical time scale is not involved in the above model because we ignored the effect of heat release on the fluid dynamic processes.

If one includes the effect of heat release via the dilatation term then

$$\widetilde{\epsilon_c} \simeq \left(1 + \frac{2}{3} C_{\epsilon_c} \frac{s_L^o}{\sqrt{\tilde{k}}} \right) \left(C_{D_c} \frac{s_L^o}{\delta_L^o} + C_D \frac{\tilde{\epsilon}}{\tilde{k}} \right) \widetilde{c''^2}, \tag{13}$$

where C_{D_c} is a constant resulting from Eq. (11) and it is the ratio of $4K_c$ to $(2C_m - 1)\beta$. The model given by Eq. (13) involves explicit dependence of the dissipation rate on the chemical time scale. It seems that the heat release occurring in the flame increases the dissipation rate in addition to the increase by the propagation mechanism. It is also interesting to note that the model for $\widetilde{\epsilon_c}$ given by Eq. (13) degenerates to the classical model if c is a nonreactive and a nonpropagative scalar. A simple algebraic expression for the mean reaction rate can now be obtained via $\overline{\dot{\omega}} = 2\overline{\rho}\widetilde{\epsilon_c}/(2C_m - 1)$ and Eq. (13). Earlier models for the mean reaction rate do not involve [7,17] the chemical time scale explicitly as obtained here.

3. DNS comparisons

In this section, DNS data sets are used to validate the algebraic model obtained above for the scalar dissipation rate. The DNS data [15,16] are in the thin flamelet combustion regime. The attributes of these data sets are given in Table 1. The case R1 [15] used complex chemical kinetic mechanism for H_2–air combustion in two-dimensional decaying turbulence under conditions where strong thermodiffusive effects occur. The case R2 [16] used a single irreversible reaction to directly simulate premixed combustion in three-dimensional spatially decaying turbulence. The data sets at $t^+ = 1.41$ and 2.59 from the case R1 are considered for analysis here. For the case R2, the data set is available only at $t^+ = 19.4$. In the above and following discussions, the quantities with superscript $+$ denote the values appropriately normalized using the planar unstrained laminar flame thickness and its burning velocity. It is worth noting that the length scale ratio given in Table 1 for the case R2 is obtained using (Λ/δ) reported in [16] and $(\delta_L^o/\delta) = 2(1+\tau)^{0.7}$ [7]. The Zeldovich thickness based on the thermal diffusivity and s_L^o is denoted by δ.

The contours of c from cases R1 and R2 are plotted in Fig. 1. Figs. 1a and 1b are from the two-dimensional simulation R1 and Figs. 1c and 1d are from the three-dimensional case R2. It is clear that the combustion in both simulations is occurring in thin regions. At a later time in the two-dimensional case the turbulent combustion may seem to be nonflamelet-like because the contours of c are nonparallel and reactant islands are formed as in Fig. 1b. Since the

Table 1
Initial parameters of direct simulation data used

Run	2D/3D	Chemistry	τ	u'/s_L^o	Λ/δ_L^o	Re	Da
R1	2D	Multistep	2.67	2.68	22.31	598	8.33
R2	3D	Single-step	2.3	1.41	6.16	56.7	4.37

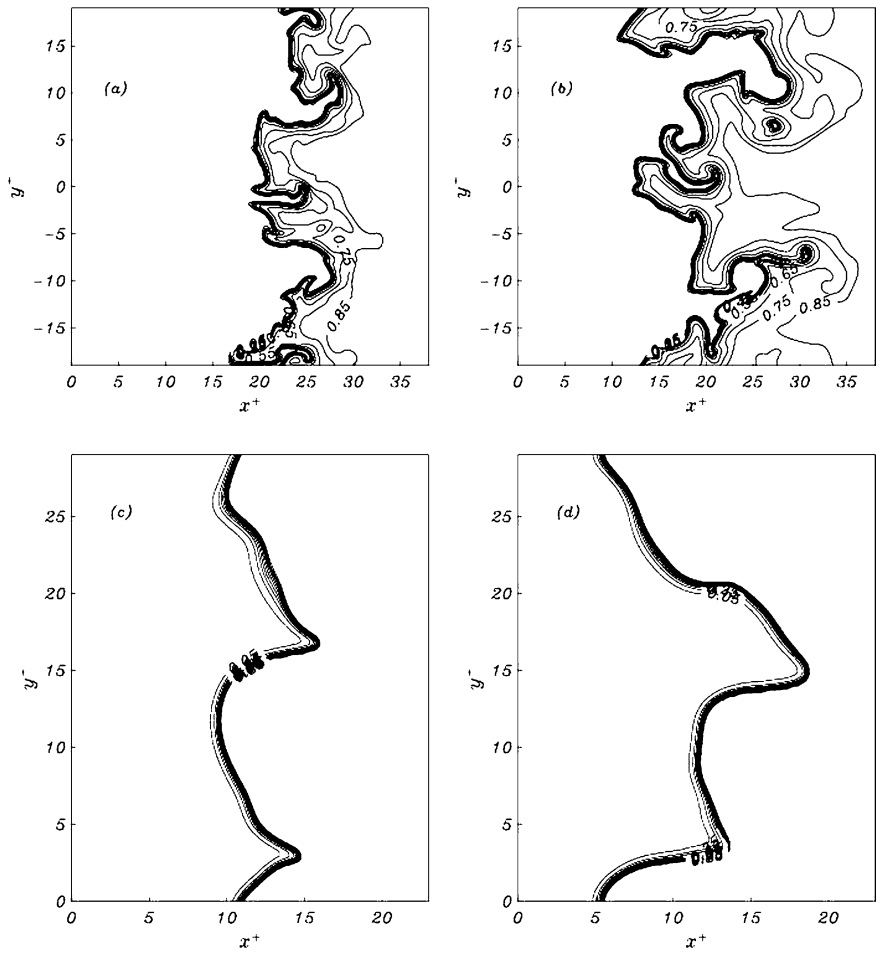

Fig. 1. Contours of progress variable, c, from the DNS data sets used. The contours are plotted from 0.05 to 0.85 with a constant interval of 0.1. Panels (a) and (b) are from the 2D case R1 at $t^+ = 1.41$ and 2.59, respectively. Panels (c) and (d) are from the 3D case R2 and they respectively represent the mid and 3/4th z plane. The domain size is normalized using the respective laminar flame thermal thickness, δ_L^o.

flame is a rich hydrogen–air flame of equivalence ratio, $\phi = 1.3$, the predominant heat release occurs in the region $c \leqslant 0.4$. For these values of c where chemical processes are dominant, one may observe that the iso-level contours are parallel to each other and closely spaced. Thus, one can see that the combustion is in thin reaction zones. This is consistent with the values of velocity and length scales ratios given in Table 1. Also, the calculation R1 was observed to be underresolved numerically in an earlier study [37]. Despite this we analyze this data set with the hope that some information about the behavior of $\widetilde{\epsilon_c}$ may be obtained. However, due care needs to be exercised while interpreting the results from this case. Here, we consider only the results which are not affected to a large extent by the numerical resolution issues. Analysis of the case R2 shows that this calculation is resolved very well.

If the turbulent combustion is in the thin flamelet regime then $\tilde{c}_{,k} \ll c''_{,k}$. Thus, from Eq. (5) one may write $\widetilde{\epsilon_c} \simeq \widetilde{N}$ for this regime of turbulent combustion. This observation is tested in Fig. 2 using the DNS data. Results from the case R1 are shifted up arbitrarily for clear presentation. The agreement is excellent for the case R2 showing the validity of the above assumption. In the case R1, the agreement between $\widetilde{N}$ and $\widetilde{\epsilon_c}$ is good except for the regions around $\tilde{c} \simeq 0.7$. A laminar hydrogen–air flame with $\phi = 1.3$ releases most of its heat around $c \simeq 0.3$ [37]. The turbulent flame in the case R1 also shows this behavior. Thus, one expects the scalar dissipation rate to peak around this location because of the strong dependence of reaction rate on the scalar dissipation rate. This can be clearly observed in Fig. 2 for the case R1. However, the second peak in $\widetilde{\epsilon_c}^+$ around $\tilde{c} \simeq 0.7$ is nonphysical

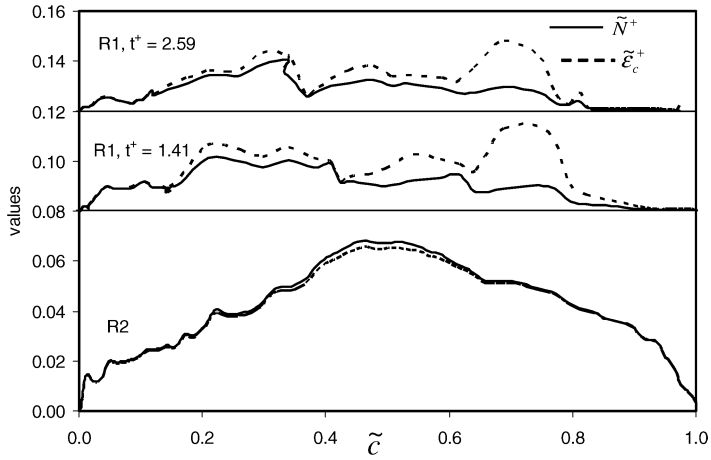

Fig. 2. Variation of $\widetilde{N}^+$ and $\widetilde{\epsilon_c}^+$ inside the flame brush in cases R1 and R2. These quantities are normalized using the respective laminar flame thermal thickness and its speed. Note that $\widetilde{N}^+$ includes the contribution from gradients of mean progress variable also (see the definition of N in the Introduction).

and is because of insufficient numerical resolution as observed in [37].

In laminar flames, the progress variable variation in the flame-normal direction follows an error function-type behavior. For this spatial variation of c, one would expect its gradient to peak at $c = 0.5$. In the case R2, one may expect a similar behavior for c since the combustion is in thin flamelets. In this regime, the behavior of the scalar dissipation rate will be dominated by the variation of the gradient of c in the flame-normal direction. Thus, the dissipation rate peaks in the middle of the flame brush. Note that the fluid properties were held constant in the DNS [16]. If the fluid properties were allowed to depend on temperature then the peak scalar dissipation rate would have shifted toward the burnt side of the flame brush as observed by Mantel and Bilger [41].

In the light of the results shown in Fig. 2, one may argue that Eqs. (6) and (7) are essentially the same for turbulent combustion in the thin flamelet regime. The differences between these equations come via terms T_{12}, T_{31}, and T_{33}. Indeed, the order of magnitude analysis presented in Appendix A shows that these terms are negligible in the thin flamelet combustion regime. Thus, one may simply replace $\widetilde{N}$ in Eq. (6) by $\widetilde{\epsilon_c}$.

The classical model for the scalar dissipation rate is $\widetilde{\epsilon_c}^+ \simeq \mathcal{R}(\widetilde{\epsilon^+}/\widetilde{k^+})\widetilde{c''^2}$, where $\mathcal{R}$ is defined to be the ratio of dissipation time scales of turbulence to scalar. Generally, this time scale ratio is assumed to be constant with a value of about 2. This model works well for a passive scalar but not for a reactive scalar like c. Mantel and Bilger [41] observed a large variation of $\mathcal{R}$ inside turbulent flame brush in their analysis of different DNS data sets. A similar behavior of $\mathcal{R}$ is also observed here as in Fig. 3. Note that $\mathcal{R}/10$ is shown in Fig. 3. The time scale ratio also seems to depend on the Re and Da (see Eq. (12)) via the ratio $s_l^o/\sqrt{\tilde{k}}$ as observed by Mantel and Borghi [12]. However, the model given by Eq. (12) is applicable only if the condition $(\sqrt{\tilde{k}}/s_l^o) > 0.067$, for $C_{\epsilon_c} = 0.1$, is met. The DNS data sets considered here satisfy this condition allowing us to test the model.

The model constant C_D in Eqs. (12) and (13) can be written as $C_D \approx \widetilde{\epsilon_c}/(\tilde{\epsilon}/\tilde{k})$. The value of C_D calculated thus varies across the flame brush as shown in Fig. 3. For further analysis of DNS data presented below, we take $C_D \approx 0.05$ which is close to the average of the variation shown in Fig. 3. Typical variation of $(\tilde{\epsilon}^+/\tilde{k}^+)$ in the turbulent flame brush is shown in Fig. 4 while the inset in Fig. 4 shows the variation of $\tilde{\epsilon}^+$. This result is from the case R2. The turbulence time scale is minimum around $\tilde{c} \simeq 0.7$ and increases on either side. Because of peak heat release around this location, the turbulent kinetic energy is maximum around this location, leading to large dissipation rate as in the inset of Fig. 4. Thus, the turbulence time scale is minimum at the location of peak heat release.

Fig. 5 compares the values of the scalar dissipation rate in the DNS data at $t^+ = 19.4$ and predicted by the three models, the classical model and those given by Eqs. (12) and (13), discussed above. The DNS results are from the case R2 and show a typical bell-shape variation seen in turbulent flame experiment [26]. The classical model with $\mathcal{R} = 2.0$ overpredicts the scalar dissipation rate. The predictions of $\widetilde{\epsilon_c}^+$ by Eqs. (12) and (13) with $C_D = 0.05$ are also shown in Fig. 5. If one uses $\mathcal{R} = 0.05$ in the classical model then the variation predicted by this model is almost close to that given by Eq. (12). These values are lower than the DNS values and the predictions are unsatisfactory. The predictions of these two models show that $\widetilde{\epsilon_c}^+$ is

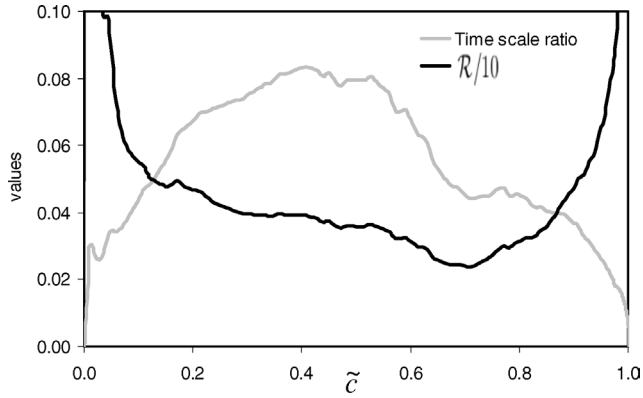

Fig. 3. Variation of time scale ratio, C_D, and the calibrated value of the classical model constant $\mathcal{R}$ inside the flame brush in the case R2. Note that $\mathcal{R}/10$ is shown.

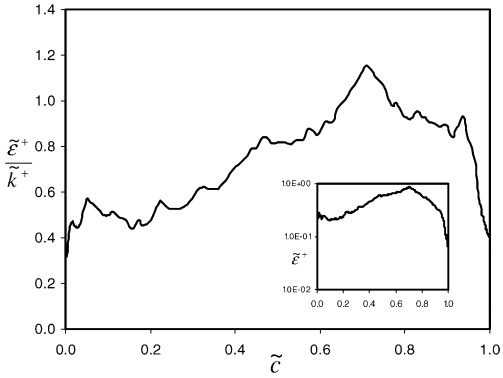

Fig. 4. Variation of the inverse of turbulence time scale inside the turbulent flame brush in case R2. The inset shows the variation of Favre mean of turbulent kinetic energy dissipation rate, $\tilde{\epsilon}^+$. The quantities are normalized by the unstrained laminar flame speed and its thermal thickness appropriately.

increasing nearly linearly inside in the flame brush up to $\tilde{c} \approx 0.7$ and then decreases on trailing side of the flame brush. In these two models, the variation of $\widetilde{\epsilon_c}$ is predominantly determined by the behavior of $(\tilde{\epsilon}/\tilde{k})$.

The prediction by the revised model, Eq. (13), developed in this study is close to the DNS value. The bell shape variation is also captured by this model. The close agreement observed between the DNS data and the revised model prediction is encouraging. Comparisons of predictions of this model with more DNS and experimental results will be interesting and useful. A systematic study of nonunity Lewis number effects will also be interesting. At least in the cases considered here, this model clearly shows that the contribution of heat release overwhelmingly dominates the contribution of the turbulence process. This implies that the scalar dissipation rate inside the turbulent flame brush is controlled by the chemical processes as envisaged by Libby and Bray [18].

Note that the direct simulation in the case R2 used a single irreversible reaction to mimic the combustion chemistry. It will be interesting to see the influence of multistep chemistry on the behavior of the revised model obtained here. Thus, the data set at $t^+ = 1.41$ from the case R1 is analyzed to obtain the variation of scalar dissipation rate across the turbulent flame brush. This is shown in Fig. 6 and the variation is similar to that given in Fig. 5 except for the peak around $\tilde{c} = 0.7$. This peak is because of the insufficient numerical resolution in the direct simulation as noted earlier. The values of scalar dissipation rate obtained via Eqs. (12) and (13) using the DNS values for $\tilde{k}$, $\tilde{\epsilon}$, and $\widetilde{c''^2}$ are also shown in Fig. 6. For this case also, we used $C_{D_c} = 0.24$ as in the previous case. However, value of C_D, which is related to the ratio of turbulence time scale to scalar time scale, and is obtained in the same manner as for data set R2, is about two orders of magnitude smaller than the value used in the previous case. This is because, the direct simulation in the case R1 is two-dimensional. The processes of turbulence kinetic energy production and its dissipation in two-dimensional flows are different from those in three-dimensional flows. Thus, obviously one may expect to have a different value for C_D in two-dimensional flows.

It is important to note that the scalar c is reactive and thus the chemical processes will also affect the dissipation of c fluctuations. This means that the chemical time scale should also be involved in the model. Such a model is derived above and is given by Eq. (13). The prediction of this model is compared to DNS values and the classical model prediction in Fig. 5. The agreement to the DNS data is improved enormously and is encouraging. However, caution needs to be exercised in interpreting the results shown in Fig. 6 because of the two-dimensionality of the DNS in the case R1. It would be interesting and worthwhile to test this model's performance using

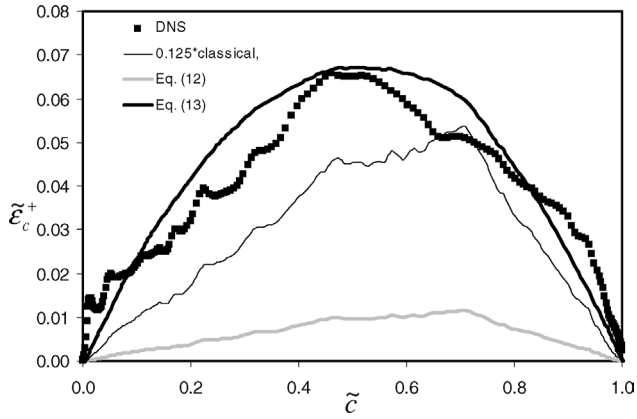

Fig. 5. Comparison of normalized predicted dissipation rate, $\widetilde{\epsilon_c}^+$, using Eq. (13) to the DNS values in case R2. Note that $\widetilde{\epsilon_c}^+/8$ is shown above for the classical model.

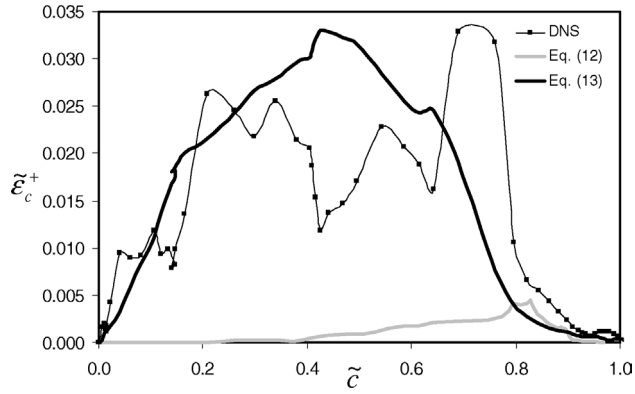

Fig. 6. Comparison of normalized predicted dissipation rate, $\widetilde{\epsilon_c}^+$, using Eq. (13) to the DNS values in 2D case R1 at $t^+ = 1.41$.

DNS data for high Re than those considered in the data sets used here and using three-dimensional DNS data with complex or reduced chemistry.

4. RANS test problem

In principle, Eq. (8) with the above models can be used for RANS calculation of turbulent premixed flames. We consider a test problem detailed below to study the effect of dilatation on the flame propagation. The test problem we consider is a statistically 1D planar turbulent flame brush propagating in a frozen turbulence field. The frozen turbulence implies that the turbulent kinetic energy and its dissipation rate remain constant in time and space. The propagation of the turbulent flame brush is unsteady and is governed by the set of equations given below.

4.1. Governing equations

The equations to be solved in RANS of turbulent premixed flames are the transport equations for the mass, the momentum, the turbulent kinetic energy, and its dissipation rate for the mean flow along with the transport equations for $\tilde{c}$ and $\widetilde{\epsilon_c}$. These equations for high Reynolds number flow can be written [38] as

$$\frac{\partial \overline{\rho}}{\partial t} + \frac{\partial \overline{\rho}\widetilde{U}}{\partial x} = 0, \tag{14}$$

$$\frac{\partial \overline{\rho}\widetilde{U}}{\partial t} + \frac{\partial \overline{\rho}\widetilde{U}\widetilde{U}}{\partial x} = -\frac{\partial \overline{P}}{\partial x} - \frac{\partial}{\partial x}\left(\widetilde{\overline{\rho}u''u''}\right), \tag{15}$$

$$\frac{\partial \overline{\rho}\tilde{k}}{\partial t} + \frac{\partial \overline{\rho}\widetilde{U}\tilde{k}}{\partial x} = \frac{\partial}{\partial x}\left[\left(\mu + \frac{\mu_t}{Sc_k}\right)\frac{\partial \tilde{k}}{\partial x}\right] - \widetilde{\overline{\rho}u''u''}\frac{\partial \widetilde{U}}{\partial x} - \overline{u''}\frac{\partial \overline{P}}{\partial x} + \overline{p'\nabla\cdot\mathbf{u}''} - \overline{\rho}\tilde{\epsilon}, \tag{16}$$

$$\frac{\partial \overline{\rho}\tilde{\epsilon}}{\partial t} + \frac{\partial \overline{\rho}\widetilde{U}\tilde{\epsilon}}{\partial x} = \frac{\partial}{\partial x}\left[\left(\mu + \frac{\mu_t}{Sc_\epsilon}\right)\frac{\partial \tilde{\epsilon}}{\partial x}\right] - C_{\epsilon 1}\overline{\rho}\frac{\tilde{\epsilon}}{\tilde{k}}\widetilde{\overline{u''u''}}\frac{\partial \widetilde{U}}{\partial x} - C_{\epsilon 1}\overline{u''}\frac{\tilde{\epsilon}}{\tilde{k}}\frac{\partial \overline{P}}{\partial x} - C_{\epsilon 2}\overline{\rho}\frac{\tilde{\epsilon}^2}{\tilde{k}}, \tag{17}$$

$$\frac{\partial \overline{\rho}\tilde{c}}{\partial t} + \frac{\partial \overline{\rho}\widetilde{U}\tilde{c}}{\partial x} = \frac{2}{(2C_m - 1)}\overline{\rho}\widetilde{\epsilon_c} - \frac{\partial \overline{\rho u''c''}}{\partial x}, \tag{18}$$

$$\frac{\partial \overline{\rho}\widetilde{\epsilon_c}}{\partial t} + \frac{\partial \overline{\rho}\widetilde{U}\widetilde{\epsilon_c}}{\partial x} = \frac{\partial}{\partial x}\left(\frac{\mu_t}{Sc_{\epsilon_c}}\frac{\partial \widetilde{\epsilon_c}}{\partial x}\right) + \frac{4K_c}{(2C_m-1)}\left(\frac{s_L^o}{\delta_L^o}\right)\overline{\rho}\widetilde{\epsilon_c} - C_{p_c}\overline{\rho}\left(\frac{\tilde{\epsilon}}{\tilde{k}}\right)\widetilde{u''c''}\frac{\partial \tilde{c}}{\partial x} + A_e\overline{\rho}\left(\frac{\tilde{\epsilon}}{\tilde{k}}\right)\widetilde{\epsilon_c} - C_{p_u}\overline{\rho}\widetilde{\epsilon_c}\frac{\widetilde{u''u''}}{\tilde{k}}\frac{\partial \widetilde{U}}{\partial x} - \frac{2}{3}\beta\overline{\rho}\frac{\widetilde{\epsilon_c}^2}{\tilde{c}(1-\tilde{c})}\left(\frac{3}{2} - C_{\epsilon_c}\frac{s_L^o}{\sqrt{\tilde{k}}}\right). \quad (19)$$

The mean density is obtained via $\overline{\rho} = \rho_u(1+\tau\tilde{c})^{-1}$. The momentum equation yields $\widetilde{U}$. The pressure, $\overline{P}$, is obtained via the continuity equation using the pressure correction approach of Patankar [39]. The turbulent kinetic energy and its dissipation rate can be obtained via Eqs. (16) and (17). Since the turbulence is assumed to be frozen in the test cases considered here, $\tilde{k}$ and $\tilde{\epsilon}$ equations are not solved. The progress variable variation is obtained from Eq. (18). The reaction rate can be closed via the $\widetilde{\epsilon_c}$ equation. In this study, we use the algebraic closure for $\widetilde{\epsilon_c}$ instead of using Eq. (19). This is to avoid the uncertainty arising because of various model constants involved in the $\widetilde{\epsilon_c}$ transport equation. Also, by using the algebraic closure for the mean reaction rate the number of equations to be solved is reduced to three (Eqs. (14), (15), and (18)).

The Reynolds stress in Eq. (15) and the turbulent scalar flux in Eq. (18) are to be modeled. The Reynolds stress is modeled [7] as $3\overline{\rho}\widetilde{u''u''} = -4\mu_t \times (\partial\widetilde{U}/\partial x) + 2\overline{\rho}\tilde{k}$. The turbulent viscosity is calculated as $\mu_t = \overline{\rho}c_\mu(\tilde{k}\tilde{k}/\tilde{\epsilon})$ following the classical $\tilde{k}$–$\tilde{\epsilon}$ turbulence closure. The turbulent scalar flux, $\widetilde{u''c''}$ is obtained using a gradient hypothesis. The use of the gradient model for the turbulent scalar flux may be questionable and it will definitely influence the flame propagation observed. As long as we keep the scalar flux model consistent between calculations with and without dilatation effect, the influence of dilatation on the flame propagation via the mixing models can be studied.

The unsteady calculations are started by initializing the computational domain with hot products on one side and cold reactants on the other side. This is achieved by specifying a variation for $\tilde{c}$ (see Fig. 8). The computational domain size is 0.25 m and contains 300 cells which are uniformly spaced. From the specified initial variation of $\tilde{c}$, the initial conditions for density and velocity are obtained. Pressure is specified to be atmospheric at the end of the computational domain. Since the turbulence is frozen, the velocity of reactant mixture coming into the domain is specified to be zero while the density of this mixture is specified to be 1.2 kg/m^3. The size of the time step used in the calculation is about a microsecond. A typical

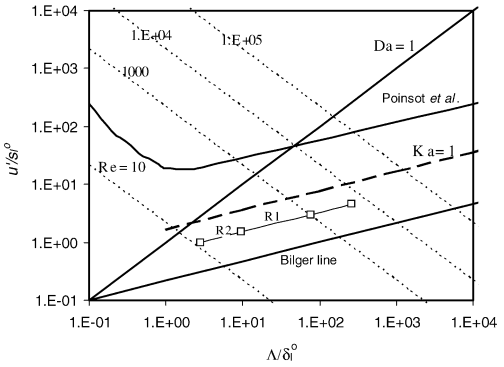

Fig. 7. Turbulent premixed combustion diagram showing the conditions of four different turbulent premixed flames considered for RANS calculation (also see Table 3). The initial conditions of the DNS data (R1 and R2) considered are also shown above.

calculation is continued until a steady flame propagation is observed and the time span for this depends on the initial turbulence level specified. The RANS calculations using the models given by Eqs. (12) and (13) are respectively referred to as EBU1 and REBU in the following discussion.

4.2. RANS results

RANS calculations of the test problem are carried out with EBU1, Eq. (12), and REBU, Eq. (13), models for the mean dissipation rate. The calculations are done for $u'/s_L^o = 1$, 1.5, 3.0, and 4.5 with $\tau = 2.3$. This value of τ implies a moderate heat release in the turbulent flame. Thus, one may expect a gradient transport for the turbulent scalar flux in the most part of the flame brush [42]. The nondimensional parameters of the flames considered here are given in Table 3 and are also marked in the turbulent combustion regime diagram shown in Fig. 7. Note that the integral length scale of the turbulence field is normalized using the laminar flame thermal thickness. The line of Karlovitz number equal to one represents the Klimov–Williams criterion for flamelet combustion. The Karlovitz number is defined as $\mathrm{Ka} \equiv (\delta/\eta_k)^2 = \{[2(1+\tau)^{0.7}]^{-1}(u'/s_L^o)^3(\delta_L^o/\Lambda)\}^{0.5}$ and is kept constant at about 0.28 for all the cases considered. It is also suggested [3] that the combustion occurs in thin flamelets if the Kolmogorov length scale $\eta_k > \delta_L^o$. One should, however, remark that the criterion defining the regimes of turbulent combustion is still an open question.

The propagation of turbulent flame brush in the case F1 is shown in Fig. 8a in the form of spatial variation of $\tilde{c}$ at various times. This flame has $u'/s_L^o = 1$. After going through some initial transients, the spatial variation of $\tilde{c}$ settles well and the flame brush travels

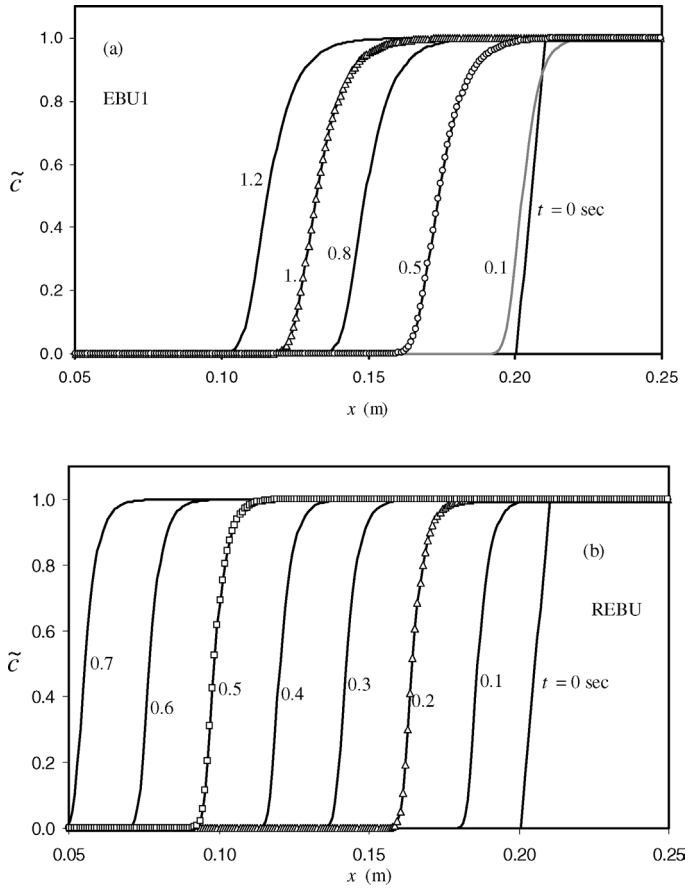

Fig. 8. Comparison of flame propagation predicted by (a) EBU1 and (b) REBU models. The unsteady premixed flame F1 is traveling from right to left in a frozen turbulence field with $u'/s_L^o = 1$ and $\Lambda/\delta_L^o = 2.86$.

toward the unburnt side at a constant speed. A number of different initial profiles were considered in a preliminary calculation and the speed of the flame brush propagation in the steady regime is found to be independent of the initial profile specified. But the initial transient period depends on the initial condition. We choose the initial profile which showed a short transient period for the calculations reported here. Also, the solutions given here are not checked for numerical grid independence. However, the grid independence of the solution is not of prime importance to address the objective of this study and it will not influence the conclusions of this investigation. To give some idea about the numerical resolution used in the calculation, locations of the grid cells are shown in Fig. 8 for few instances.

The flame is propagating faster as in Fig. 8b when the effect of heat release is included. By about $t = 0.7$ s, the turbulent flame brush is very close to the left boundary of the computational domain. Whereas in Fig. 8a, the flame brush is still well within the computational domain even at $t = 1.2$ s. In addition to the faster propagation, the spatial variation of $\tilde{c}$ becomes steep causing the numerical resolution to deteriorate slightly. This becomes more obvious near the cold front of the flame brush. It is observed that the numerical resolution becomes worse if a countergradient transport model for the turbulent scalar flux is used. This is the main reason for us to choose a moderate value for τ and gradient flux model for the turbulent scalar flux in this study. However, the issue on numerical resolution can be solved if one follows an adaptive griding technique which will be used in future investigations.

It is easy to calculate the displacement speed, S_d, from the time trace of a particular value of $\tilde{c}$. In the thin flamelet combustion regime, all the iso-contours of c move at the same displacement speed. Indeed, such a behavior is observed by plotting (not shown) the loci of $\tilde{c} = 0.3$, 0.5, and 0.7 with time. Thus, it is immaterial which value of $\tilde{c}$ is chosen to calculate S_d. Here, we choose $\tilde{c} = 0.5$ to calculate the displacement speed. The time trace of $\tilde{c} = 0.5$ is shown in Fig. 9 for various cases considered here. The three cases in

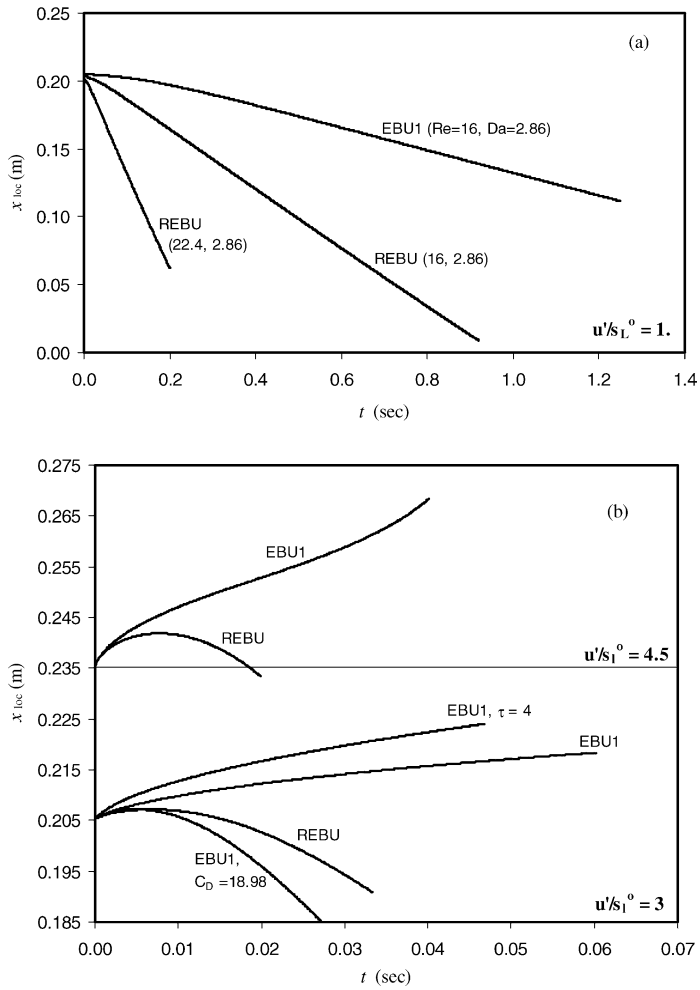

Fig. 9. The time trace of $\tilde{c} = 0.5$ in various test flames considered for RANS calculation. Panel (a) shows the results for $u'/s_L^o = 1$ case, flame F1 in Table 3, and panel (b) shows the results for $u'/s_L^o = 3$ and 4.5, flames F3 and F4. This figure clearly shows the importance of the dilatation term. The positive slope of the curves in (b) indicates the flame blowoff: inability of the flame brush to propagate into the unburnt mixture.

Fig. 9a are represented by the first square (southwest to R2) in Fig. 7. After an initial short transient period, there is a linear decrease of x_{loc} with t in all the cases shown in Fig. 9a. The slope of this linear variation yields the displacement speed. It is clear from Fig. 9a that including the effect of heat release increases the displacement speed by nearly two and half times (compare the curves marked REBU and EBU1 for the same values of Re and Da).

The unstrained laminar flame speed and its thermal thickness will change when the stoichiometry of the unburnt mixture is changed. To understand the capability of the models to capture this effect, for the case with Re = 22.4 in Fig. 9a we used a value for unstrained laminar flame speed which is about three times larger than the values used in the other cases and the laminar flame thermal thickness which is half the value used in the other cases with $u'/s_L^o = 1$. Although the values of u'/s_L^o and Λ/δ_L^o are kept to be the same as in the other two cases in Fig. 9a, the displacement speed changes when the mixture stoichiometry is changed. This observation is well known. The difference between the predictions of EBU1 and REBU models for the flame with Re = 22.4 is similar to the other case shown in Fig. 9a. One should note that the same values of the model constants given in Table 2 are used.

One can apply the KPP analysis [43] to predict the turbulent flame speed in the test problem considered here. According to this analysis the turbulent flame speed is given by $S_T = 2\sqrt{\nu_t/(\rho_u Sc_c)(\partial\overline{\dot{\omega}}/\partial\tilde{c})_{\tilde{c}\to 0}}$.

Table 2
Model constants used in RANS calculation

Equation	Const. and value								
Flow	C_μ	Sc_k	Sc_ϵ	$C_{\epsilon 1}$	$C_{\epsilon 2}$				
	0.09	1.0	1.3	1.44	1.92				
Scalar	Sc_c	Sc_{ϵ_c}	C_m	K_c	A_e	β	C_{ϵ_c}	C_{p_c}	C_{p_u}
	1.0	1.3	0.7	0.1	0.9	4.2	0.1	1.0	1.0

Table 3
Characteristics of turbulent flames considered in RANS calculation

Flame	u'/s_L^o	Λ/δ_L^o	Re	Da	Ka
F1	1.0	2.8	16	2.9	0.28
F2	1.5	9.6	81	6.4	0.28
F3	3.0	77.1	1300	25.7	0.28
F4	4.5	260.4	6560	57.9	0.28

All the flames listed above are calculated with both EBU1 and REBU models respectively given by Eqs. (12) and (13).

Thus, one can write

$$\frac{S_T^{\mathrm{REBU}}}{S_T^{\mathrm{EBU1}}} = \left[1 + \frac{3C_{D_c}}{2C_D}\frac{(\Lambda/\delta_L^o)}{(u'/s_L^o)}\right]^{1/2}$$

using the models EBU1 and REBU described above for the mean reaction rate. The turbulence in the cold reactant is taken to be isotropic. For the values given in Tables 2 and 3, one gets the above ratio to be 2.4 for $u'/s_l^o = 1$. The numerical calculation gives about 2.7. For $u'/s_l^o = 3$, a graphical extrapolation of the results in Fig. 9b yields $S_T^{\mathrm{REBU}}/S_T^{\mathrm{EBU1}} \approx 0.5$ whereas the KPP analysis gives 0.7, with $C_D = 18.98$ in EBU1 model.

Fig. 9b shows the variation of $\tilde{c} = 0.5$ locus with time in the other, F3 and F4, flames considered for RANS simulation. The two filled squares on the northeast side of R1 in Fig. 7 represent these two turbulent flames. There are a number of cases in Fig. 9b. The bottom and top parts respectively show the predictions of flames F3 and F4. Both the EBU1 and REBU models are used. The results for the F4 flame is shifted arbitrarily for a clear presentation. The most striking feature in Fig. 9b is that the turbulent flame does not show any propagation toward unburnt mixture when the model EBU1 is used. This is signified by the positive slope of the curve marked EBU1. Even by changing the value of heat-release parameter, τ, to four (higher heat release) the EBU1 model is unable to predict flame propagation. This is because the mean reaction rate predicted by the EBU1 model is small compared to the turbulent convective and diffusive rates in Eq. (18). The reduced mean chemical rate modifies the flame propagation problem to a simple convective–diffusive problem. Thus, the turbulent flame brush is pushed downstream by the turbulence processes leading to flame blowoff.

If one increases the value of the model constant C_D to about 19 via $C_D = [C_{D_c} s_L^o/\delta_L^o + A_e\tilde{\epsilon}/(\beta\tilde{k})]/(\tilde{\epsilon}/\tilde{k})$ then the propagation of the flame brush is observed as in Fig. 9b. This case is marked as (EBU1, $C_D = 18.98$) in Fig. 9b. However, if the effect of heat release is included via the REBU model then the propagation of the turbulent flame brush is observed with no changes to model constants as depicted in Fig. 9b. Similar behavior is observed in the flame F4 also. The flame blowoff, however, seems to be more dramatic in the flame F4 because of high turbulent convective and diffusive rates. From Fig. 9, one can clearly see the importance of the dilatation term T_2.

It is also interesting to study the structure of the flame brush structure predicted by the EBU1 and the REBU models. This is shown in Fig. 10 in the form of spatial variation of $\tilde{c}$ which is taken after a steady propagation is established. The spatial location where $\tilde{c} = 0.5$ is denoted by x^*. To assist proper comparison, the spatial coordinate is shifted so that the origin is in the middle of the corresponding flame brush. The shifted spatial coordinate is normalized using the corresponding value of the laminar flame thermal thickness. As one can observe in Fig. 10, including the effects of heat release makes the flame brush thin. This is because of increased mixing rate leading to an increase in the reaction rate. The decrease in the flame brush thickness is consistent with the variations observed in Figs. 8 and 9. When u'/s_L^o is increased, the turbulent flame brush becomes thick as in Fig. 10. The structure of the flame brush predicted by the EBU1 model for high u'/s_L^o is not shown in Fig. 10 because this model is unable to predict a propagating flame brush with no modification to the model constant, C_D.

5. Summary and conclusion

Exact transport equations for the instantaneous scalar dissipation rate, N, and its Favre mean, $\widetilde{N}$, are derived from the transport equation for the instantaneous progress variable, c. When the turbulent combustion is taken to occur in thin flamelets, the contribution of the gradient of mean progress variable to $\widetilde{N}$ is negligible and the mean scalar dissipation rate, $\widetilde{\epsilon_c}$, represents the dissipation of the progress variable variance. A transport equation for $\widetilde{\epsilon_c}$ is also obtained. This exact equation is closed using models derived in earlier studies, together with the Bray–Moss–Libby approach, which is used to obtain a closure for the contribution of the dilatation.

An order of magnitude analysis of the $\widetilde{\epsilon_c}$ transport equation identifies the dominant terms when the tur-

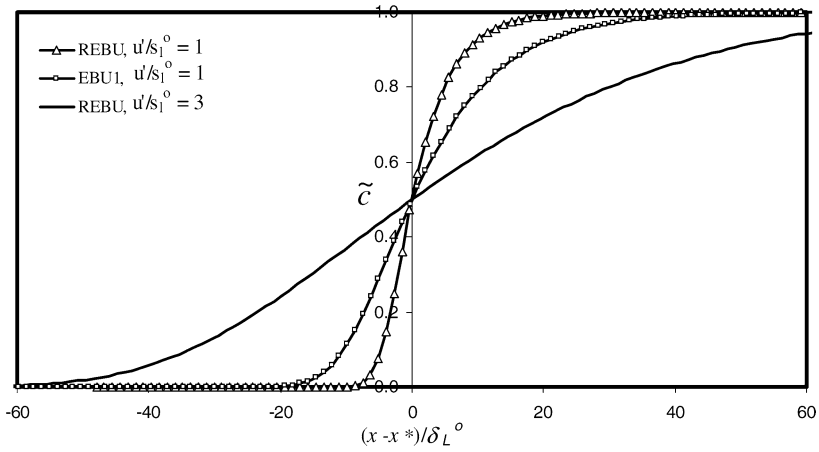

Fig. 10. The structure of turbulent flame brush predicted by EBU1 and REBU models. For large values of u'/s_L^o, EBU1 is unable to predict a propagating turbulent flame brush and thus it is not shown above.

bulence Reynolds and Damköhler numbers are large. The scalings used in the order of magnitude analysis are verified by analyzing DNS data of turbulent premixed flame depicting the characteristics of thin flamelet combustion. The order of magnitude analysis shows that the strain, the dissipation, the dilatation, and the chemical reaction terms are the dominant terms. Using these terms, a simple algebraic closure for the mean scalar dissipation rate is obtained. The closure model obtained here involves an appropriate chemical time scale as well as a turbulence time scale and retains the coupling between the chemical and diffusive processes in turbulent premixed flames. Earlier models for the mean scalar dissipation rate used in turbulent premixed flame calculations involve only a turbulence time scale. If the scalar c is set to be a nonreactive and nonpropagative scalar then the model derived here degenerates to the well-known classical model for the mean scalar dissipation rate. The mean scalar dissipation rate predicted by the model obtained here compares well with the DNS data.

The effect of dilatation on the propagation of turbulent flame is also studied via RANS calculation of a simple test problem. The test problem considered is a statistically one-dimensional planar turbulent flame propagating in a frozen turbulence field. RANS simulation of this test flame is conducted using a finite volume method. These calculations show that including the effect of dilatation increases the displacement speed by nearly three times when $u'/s_L^o = 1$. For this case, the flame brush is found to be thin when the heat-release effects are included in the model for the mean scalar dissipation rate.

For high values of u'/s_L^o, including the effect of dilatation in the mixing model is crucial for predicting the flame propagation. The models for the mean scalar dissipation rate obtained from the analysis of the incompressible flows lead to flame blowoff unless the model constant C_D is changed by an order of magnitude.

Acknowledgments

We thank Drs. T. Poinsot and B. Cuenot of CERFACS and Dr. R.S. Cant and Mr. P. Vishnavi for their help in making the DNS data sets available for this study.

Appendix A

The order of magnitude analysis of Eq. (7) is carried out as follows. The spatial derivatives of mean quantities, time derivative, and density are scaled by the turbulence integral length scale, Λ, Λ/u', and ρ_u, respectively. The mean velocity and thermal diffusivity of the mixture are scaled respectively by some reference velocity U_{ref} and the laminar flame scales $(s_L^o \delta_L^o)$. The quantities involving or multiplied by the gradient of progress variable are also scaled with laminar flame quantities. This is because the gradient of the progress variable is nonzero only inside the thin flame. Using these scaling quantities and the definition of Re and Da given in Section 2.2, one obtains

$$\frac{\partial \overline{\rho}\widetilde{\epsilon_c}}{\partial t} \simeq \mathcal{O}\left(\rho_u \frac{u' s_L^o}{\Lambda \delta_L^o}\right) = \mathcal{O}\left(\rho_u \left(\frac{s_L^o}{\delta_L^o}\right)^2; \mathrm{Da}^{-1}\right),$$

$$\frac{\partial \overline{\rho}\widetilde{U}_j \widetilde{\epsilon_c}}{\partial x_j} \simeq \mathcal{O}\left(\rho_u \frac{U_{\text{ref}} s_L^o}{\Lambda \delta_L^o}\right) = \mathcal{O}\left(\rho_u \left(\frac{s_L^o}{\delta_L^o}\right)^2; (\mathrm{Da}\, u'/U_{\text{ref}})^{-1}\right),$$

$$\frac{\partial}{\partial x_j}\left(\overline{\rho\alpha}\frac{\widetilde{\epsilon_c}}{\partial x_j}\right) \simeq \mathcal{O}\left(\rho_u\left(\frac{s_L^o}{\Lambda}\right)^2\right) = \mathcal{O}\left(\rho_u\left(\frac{s_L^o}{\delta_L^o}\right)^2;(\mathrm{Re\,Da})^{-1}\right),$$

$$\overline{\rho\alpha\alpha\left(\frac{\partial c_k''}{\partial x_j}\frac{\partial c_k''}{\partial x_j}\right)} \simeq \mathcal{O}\left(\rho_u\left(\frac{s_L^o}{\delta_L^o}\right)^2\right) = \mathcal{O}\left(\rho_u\left(\frac{s_L^o}{\delta_L^o}\right)^2;1\right),$$

$$T_{11} = \frac{\partial}{\partial x_j}\overline{\rho u_j''\widetilde{\epsilon_c}} \simeq \mathcal{O}\left(\rho_u\frac{u's_L^o}{\Lambda\delta_L^o}\right) = \mathcal{O}\left(\rho_u\left(\frac{s_L^o}{\delta_L^o}\right)^2;\mathrm{Da}^{-1}\right),$$

$$T_{12} = 2\overline{\rho\alpha}\widetilde{(u_j''c_{,k}'')}\frac{\partial\tilde{c}_{,k}}{\partial x_j} \sim \mathcal{O}\left(\rho_u\left(\frac{s_L^o}{\Lambda}\right)^2\right) = \mathcal{O}\left(\rho_u\left(\frac{s_L^o}{\delta_L^o}\right)^2;(\mathrm{Re\,Da})^{-1}\right),$$

$$T_2 = 2\overline{\rho\epsilon_c(\partial u_l/\partial x_l)} \simeq \mathcal{O}\left(\rho_u\left(\frac{s_L^o}{\delta_L^o}\right)^2\right) = \mathcal{O}\left(\rho_u\left(\frac{s_L^o}{\delta_L^o}\right)^2;1\right),$$

$$T_{31} = \overline{\rho\alpha}\frac{\partial\tilde{c}}{\partial x_j}\widetilde{\left(\frac{\partial c''}{\partial x_k}\frac{\partial u_j''}{\partial x_k}\right)} \simeq \mathcal{O}\left(\rho_u\frac{{s_L^o}^2}{\Lambda\delta_L^o}\right) = \mathcal{O}\left(\rho_u\left(\frac{s_L^o}{\delta_L^o}\right)^2;(\mathrm{Re\,Da})^{-1/2}\right),$$

$$T_{32} = 2\overline{\rho\alpha}\widetilde{\left(\frac{\partial c''}{\partial x_j}e_{jk}''\frac{\partial c''}{\partial x_k}\right)} \simeq \mathcal{O}\left(\rho_u\left(\frac{s_L^o}{\delta_L^o}\right)^2\right) = \mathcal{O}\left(\rho_u\left(\frac{s_L^o}{\delta_L^o}\right)^2;1\right),$$

$$T_{33} = 2\overline{\rho\alpha}\widetilde{\left(\frac{\partial c''}{\partial x_j}\frac{\partial c''}{\partial x_k}\right)}\widetilde{e_{jk}} \simeq \mathcal{O}\left(\rho_u\frac{U_{\mathrm{ref}}s_L^o}{\Lambda\delta_L^o}\right) = \mathcal{O}\left(\rho_u\left(\frac{s_L^o}{\delta_L^o}\right)^2;(\mathrm{Da}\,u'/U_{\mathrm{ref}})^{-1}\right),$$

$$T_4 = 2\left(\overline{\alpha\frac{\partial c''}{\partial x_k}\frac{\partial\dot{\omega}''}{\partial x_k}}\right) \simeq \mathcal{O}\left(\rho_u\left(\frac{s_L^o}{\delta_L^o}\right)^2\right) = \mathcal{O}\left(\rho_u\left(\frac{s_L^o}{\delta_L^o}\right)^2;1\right).$$

References

[1] K.N.C. Bray, Proc. R. Soc. London Ser. A 431 (1990) 315–335.
[2] K.N.C. Bray, P.A. Libby, J.B. Moss, Combust. Flame 61 (1985) 87–102.
[3] R.W. Bilger, in: T. Takeno (Ed.), Turbulence and Molecular Processes in Combustion, Elsevier Science, Amsterdam, 1993, pp. 267–285.
[4] K.N.C. Bray, N. Peters, in: P.A. Libby, F.A. Williams (Eds.), Turbulent Reacting Flows, Academic Press, San Diego, 1994, pp. 63–113.
[5] K.N.C. Bray, P.A. Libby, in: P.A. Libby, F.A. Williams (Eds.), Turbulent Reacting Flows, Academic Press, San Diego, 1994, pp. 116–151.
[6] D. Veynante, L. Vervisch, Prog. Energy Combust. Sci. 28 (2002) 193–266.
[7] T.J. Poinsot, D. Veynante, Theoretical and Numerical Combustion, Edwards, Philadelphia, 2001.
[8] F.E. Marble, J.E. Broadwell, The coherent flame model for turbulent chemical reactions, Project Squid Tech. Rep. TRW-9-PU, 1977.
[9] S.B. Pope, Int. J. Eng. Sci. 26 (5) (1988) 445–469.
[10] S.M. Candel, T.J. Poinsot, Combust. Sci. Technol. 70 (1990) 1–15.
[11] R. Borghi, Combust. Flame 80 (1990) 304–312.
[12] T. Mantel, R. Borghi, Combust. Flame 96 (1994) 443–457.
[13] R. Borghi, D. Dutoya, Proc. Combust. Inst. 17 (1978) 235–244.
[14] A. Mura, R. Borghi, Combust. Flame 133 (2003) 193–196.
[15] M. Baum, T.J. Poinsot, D.C. Haworth, N. Darabiha, J. Fluid Mech. 281 (1994) 1–32.
[16] C.J. Rutland, R.S. Cant, in: Proc. of the Summer Program, Center for Turbulence Research, NASA Ames/Stanford University, Stanford, CA, 1994, p. 75.
[17] K.N.C. Bray, in: P.A. Libby, F.A. Williams (Eds.), Turbulent Reacting Flows, Springer-Verlag, New York, 1980, pp. 115–183.
[18] P.A. Libby, K.N.C. Bray, Combust. Flame 39 (1980) 33–41.
[19] R.W. Bilger, Combust. Sci. Technol. 13 (1976) 155.
[20] N. Peters, Proc. Combust. Inst. 21 (1986) 1231.
[21] S.B. Pope, Proc. Combust. Inst. 23 (1990) 591–612.
[22] A.Y. Klimenko, R.W. Bilger, Prog. Energy Combust. Sci. 25 (1999) 595–687.
[23] P.A. Libby, F.A. Williams, in: P.A. Libby, F.A. Williams (Eds.), Turbulent Reacting Flows, Academic Press, San Diego, 1994, pp. 1–62.
[24] Y.-C. Chen, M.S. Mansour, Combust. Sci. Technol. 126 (1997) 291.
[25] S.H. Starner, R.W. Bilger, M.B. Long, J.H. Frank, D.F. Marran, Combust. Sci. Technol. 129 (1997) 141.
[26] F. O'Young, R.W. Bilger, Combust. Flame 109 (1997) 683–700.
[27] Y.-C. Chen, Mansour. Proc. Combust. Inst. 27 (1998) 811.
[28] A. Soika, F. Dinkelacker, A. Leipertz, Proc. Combust. Inst. 27 (1998) 785.
[29] Y.-C. Chen, R.W. Bilger, Combust. Flame 131 (2002) 400–435.
[30] N. Swaminathan, R.W. Bilger, Combust. Theory Modelling 5 (2001) 429–446.
[31] J.L. Lumley, B. Khajeh-Nouri, Adv. Geophys. 18 (1974) 169–192.
[32] O. Zeman, J. Lumley, J. Atmos. Sci. 44 (1976) 1974–1988.

[33] W.P. Jones, P. Musonge, Phys. Fluids 31 (1988) 3589–3604.
[34] R.N. Paul, K.N.C. Bray, Proc. Combust. Inst. 26 (1996) 259.
[35] T. Mantel, in: Annual Research Briefs, Center for Turbulence Research, Stanford University, 1993, pp. 219–228.
[36] N. Swaminathan, in: Book of Abstracts, 8th International Conference on Numerical Combustion, SIAM, Amelia Island, FL, 2000, p. 44.
[37] N. Swaminathan, R.W. Bilger, B. Cuenot, Combust. Flame 126 (2001) 1764–1779.
[38] K.N.C. Bray, M. Champion, P.A. Libby, Combust. Flame 91 (1992) 165–186.
[39] S.V. Patankar, Numerical Heat Transfer and Fluid Flow, Taylor & Francis, London, 1980, pp. 113–137.
[40] D. Bradley, P.H. Gaskel, X.J. Gu, Combust. Flame 96 (1994) 221–248.
[41] T. Mantel, R.W. Bilger, Combust. Sci. Technol. 110–111 (1995) 393–417.
[42] P.A. Libby, K.N.C. Bray, AIAA J. 19 (1981) 205–213.
[43] Ya.B. Zeldovich, G.I. Barenblatt, V.B. Librovich, G.M. Makhviladze, The Mathematical Theory of Combustion and Explosions, translated from Russian by D.H. McNeill, Consultants Bureau, New York, 1985, pp. 278–286.